JPET Fast Forward. Published on April 13, 2018 as DOI: 10.1124/jpet.117.247262
This article has not been copyedited and formatted. The final version may differ from this version.

JPET #247262

NOX4 deletion in male mice exacerbates the effect of ethanol on trabecular bone and osteoblastogenesis

James Watt, Alexander W. Alund*, Casey F. Pulliam, Kelly E. Mercer, Larry J. Suva, Jin-Ran Chen, Martin J.J. Ronis+

Author Affiliations:

JW, CP, MR: Department of Pharmacology and Experimental Therapeutics, Louisiana State University Health Sciences Center, New Orleans, LA

AA: Interdisciplinary Biological Sciences Program, University of Arkansas for Medical Sciences, Little Rock, AR, * Current address: PinPoint Testing, Little Rock, AR

KEM, JRC: Department of Pediatrics, University of Arkansas for Medical Sciences, Arkansas Children's Nutrition Center, Little Rock, AR

LJS: Department of Veterinary Physiology & Pharmacology, Texas A&M University, College Station, TX

Running title: NOX4 deletion and ethanol suppress osteogenesis

+Corresponding author: Martin J.J. Ronis, PhD. Department of Pharmacology & Experimental Therapeutics, LSUHSC – New Orleans, 1901 Perdido Str., New Orleans, LA 70112.

Phone: (504) 568-4514

Fax: (504) 568-4740

Email: mronis@lsuhsc.edu

Number of text pages: 36

Number of tables: 2

Number of figures: 6

Number of references: 44

Number of words

Abstract: 249

Introduction: 745

Discussion: 1,497

Nonstandard abbreviations:

NOX4: Nicotinamide adenine dinucleotide phosphate (NADPH) oxidase-4; NOX2: Nicotinamide adenine dinucleotide phosphate (NADPH) oxidase-2; ROS: reactive oxygen species: EtOH: ethanol

Recommended section assignment: Cellular and molecular; toxicology

Abstract

Chronic alcohol consumption increases bone resorption and decreases bone formation. A major component of ethanol (EtOH) pathology in bone is the generation of excess reactive oxygen species (ROS). The ROS-generating NADPH oxidase 4 (NOX4) is proposed to drive much of the EtOH-induced suppression of bone formation. Here, 13-week old male WT and NOX4 -/- mice were pair-fed (PF) a high fat (35%) Lieber-DeCarli liquid diet with or without EtOH at 30% of their total calories for 12 weeks. Micro-CT analysis demonstrated significant decreases in trabecular bone volume/total volume (BV/TV%) and cortical thickness in WT, EtOH-fed mice compared to pair-fed (PF) controls. EtOH-fed NOX4 -/- mice also displayed decreased trabecular bone volume/total volume and trabecular number compared to PF ($p<0.05$). However, NOX4 -/- mice were protected against EtOH-induced decreases in cortical thickness ($p<0.05$) and decreases in collagen1 and osteocalcin mRNA expression in cortical bone ($p<0.05$). In WT and NOX4 -/- vertebral bone, ethanol suppressed expression of Wnt signaling components that promote osteoblast maturation. A role for NOX4 in EtOH inhibition of osteoblast differentiation was further demonstrated by protection against EtOH inhibition of osteoblastogenesis in *ex-vivo* bone marrow cultures from NOX4 -/-, but not $p47^{phox}$ -/- mice lacking active NOX2. However, bone marrow cultures from NOX4 -/-mice formed fewer osteoblastic colonies compared to WT cultures ($p<0.05$), suggesting a role for NOX4 in the maintenance of mesenchymal progenitor cell populations. These data suggest that NOX4 deletion is partially protective against EtOH effects on osteoblast differentiation, but may predispose bone to osteogenic impairments.

Introduction

Adult bone health is maintained by coordinated activities of bone resorption and bone formation, a process termed remodeling. Following osteoclastic bone resorption, pre-osteoblasts from the mesenchymal lineage infiltrate the resorbed surface and mature into osteoblasts (Martin and Seeman 2008). Osteoblast maturation is characterized by the Runx2-dependent expression of alkaline phosphatase along with expression of factors including osteocalcin and collagen 1a1 (Komori *et al.*, 1997, Long, 2011). Remodeling osteoblasts predominately lie along the trabecular network of long bone (e.g. tibia and femur) metaphyses, but also generate bone on the periosteal (outer) surface to increase bone width (Orwoll, 2003). During mineralization, these cells become entrapped within the mineralized compartment and further mature into osteocytes that orchestrate bone turnover (Dallas and Bonewald, 2010). Disruptions in osteoblast maturation decrease bone mass (Komori *et al.*, 1997; Rzonca *et al.*, 2004), resulting in pathologies such as osteopenia or osteoporosis (Poole and Compston, 2006).

The canonical Wnt pathway promotes osteoblast differentiation and osteogenesis (Duan and Bonewald, 2016). Suppression of glycogen synthase kinase 3-beta (GS3Kb) by the Frizzled receptor/LRP-5/6 receptor complex prevents degradation of beta-catenin, allowing beta-catenin to induce TCF-dependent transcriptional activity, specifically Runx2 activation (Long, 2011; Duan and Bonewald, 2016). Disruption of this pathway can perturb the balance of resorption and formation to decouple bone remodeling and thereby damage bone (Chen *et al.*, 2009; Shankar *et al.*, 2008; Shankar *et al.*, 2006; Alund *et al.*, 2017).

Increases in oxidative stress are associated with decreased rates of bone formation and Wnt antagonism (Almeida *et al.*, 2007a; Almeida *et al.*, 2007b;). Osteoblasts express NADPH oxidases 2 and 4 (NOX2 and NOX4), which generate reactive oxygen species (ROS) exclusively

(Bedard and Krause, 2007; Schroder, 2015). NOX2 is a plasma membrane-bound enzyme that generates superoxide radical, which can be converted to hydrogen peroxide by superoxide dismutase (Bedard and Krause, 2007). The constitutively active NADPH oxidase 4 (NOX4) generates hydrogen peroxide, with NOX4 activity highly correlated with expression (Brandes *et al.*, 2014). Additional data suggest that these enzymes mediate ROS-dependent activation of different intracellular signaling pathways involving members of the MAP kinase cascade (Chen *et al.*, 2008). Osteoblast precursors and mature osteoblasts express high levels of NOX4 mRNA transcripts, suggesting an influential role for NOX4 in regulation of osteoblastogenesis and osteoblast function (Ambe *et al.*, 2014; Mercer *et al.*, 2014).

Alcohol (ethanol; EtOH) adversely targets bone (Gaddini *et al.*, 2016). Reductions in bone formation by EtOH have been reported in both human and experimental studies (Nyquist *et al.*, 1996; Mercer *et al.*, 2014, Chen *et al.*, 2010). Heavy alcohol use is directly associated with lower bone mineral density and increased fracture risk (Santori *et al.*, 2008; González-Reimers *et al.*, 2011). In animal studies, co-administration of the antioxidant glutathione precursor N-acetyl cysteine reverses ethanol's disruption of bone turnover, including the suppression of the Wnt pathway and osteogenic lineage commitment, implicating oxidative stress in EtOH's mechanism of action (Chen *et al.*, 2010, 2011). In addition to suppressing bone formation, EtOH induces RANKL expression by producing excess ROS, thereby stimulating osteoclast differentiation and promoting resorption (Bai *et al.*, 2005; Chen *et al.*, 2006). Although bone loss can occur from an imbalance favoring either aspect of turnover, studies have found EtOH to suppress osteogenesis while promoting resorption (e.g. Yang *et al.* 2014, Mercer *et al.*, 2014, Callaci *et al.*, 2009). The direction of the uncoupling turnover can be model specific and dependent on physiological status. For example, males and cycling females appear to be more susceptible to osteoclastogenic

effects of EtOH due to lack of estrogen, whereas pregnant and post-lactating female rats displayed only decreased bone formation markers (Shankar *et al.* 2006, 2008). The pro-osteoclastogenic mechanism of EtOH is dependent on NOX2 activity: loss of functional NOX2, via knockout of the essential component $p47^{phox}$, prevented the RANKL induction and osteoclastogenesis (Mercer *et al.*, 2014). However, even in the absence of functional NOX2, EtOH suppressed osteoblast-mediated bone formation in mice (Mercer *et al.*, 2014), yet the pan-NOX inhibitor diphenyleneiodonium (DPI) blocked EtOH inhibition of bone formation in the rat (Chen *et al.* 2011). Given the finding that EtOH's suppression of bone formation is NOX2-independent, and NOX4's complimentary role in ROS generation in bone, we hypothesized that NOX4 is instrumental in suppressing osteoblast differentiation and/or function in response to EtOH. The studies described herein employed global NOX4 deletion in male mice to determine NOX4's contribution to the reduction in bone quality induced by EtOH. In particular, EtOH-mediated changes in long bone microarchitecture, bone formation, and osteoblast maturation via antagonism of the Wnt pathway.

Methods

Animals

All experimental procedures involving the use of animals were approved by the Institutional Animal Care and Use Committee (IACUC) at the University of Arkansas for Medical Sciences (UAMS) and the IACUC at Louisiana State University Health Sciences Center, New Orleans. Mice were housed in animal facilities approved by the Association Assessment and Accreditation of Laboratory Animal Care. 13-week old male C57Bl/6J mice (Jackson Laboratories, Bar Harbor, ME) and NOX4 -/- mice (B6.129-*NOX4*^{tm1Kkr}/J, Jackson Labs) were

JPET Fast Forward. Published on April 13, 2018 as DOI: 10.1124/jpet.117.247262
This article has not been copyedited and formatted. The final version may differ from this version.

randomized to two groups and received either a 5% v/v Ethanol liquid diet (equaling 30% of total caloric intake) or a calorically matched pair-fed control using the Leiber-DeCarli liquid diet (35% of energy from fat, 18% from protein, 47% from carbohydrates; #710260, Bethlehem, PA). Additional NOX4 -/- mice were given a standard rodent chow diet (Supplemental Figures 2 and 3). Ethanol (EtOH) was added to the Leiber-DeCarli diet by substituting carbohydrate calories until 30% total calories from ethanol was reached (Alund *et al.,* 2016). This concentration was maintained for the 84 days of the experiment until sacrifice. Calorically matched pair-fed feeding volumes were based on the previous day's consumption by the EtOH group. No significant rate of mortality was noted during the treatment phase. The final N for each group was as follows: WT PF: 4; WT EtOH: 5; NOX4 -/- PF: 5; NOX4 -/- EtOH: 6; NOX4 -/- chow: 4. At sacrifice, right and left femurs as well as vertebrae were harvested and frozen for total RNA extraction. The right tibias were fixed in 10% formalin for micro-computed tomography (micro-CT) analysis; left tibias were fixed in ethanol for histological staining and dynamic histomorphometry analysis and histological staining as described (Rzonca *et al.*, 2004). Bone marrow mesenchymal stromal cells extracted from male C57Bl6/J, from NOX4 -/- mice, and from p47phox -/- mice (B6N.129S2-*Ncf1*^{tm1Shl}/J, Jackson Labs) aged 9-10 weeks were used for *ex-vivo* osteoblast colony formation assays as described below.

Micro-computed tomography (micro-CT)

Formalin-fixed tibiae were imaged using high-resolution microcomputed tomography (micro-CT) according to current guidelines for the assessment of bone microarchitecture (Bouxsein *et al*., 2010). Right tibias were scanned using a Scanco MicroCT 40 (Scanco Medical AG, Brüttisellen, Switzerland) at 12 um voxel resolution. The trabecular compartment included a 2.8 mm region extending distally 1.24 mm from the primary spongiosa. All data were acquired at 70

kVp, 114 mA, and 200 ms integration time. The cancellous bone region was obtained in a blinded manner using a semi-automated contouring program that separated cancellous from cortical bone. Bone volume fraction (BV/TV, %), trabecular thickness (Tb.Th, mm), trabecular separation (Tb.Sp, mm), and trabecular number (Tb.N, 1/mm) were calculated using previously published methods (Suva *et al*., 2008). For cortical bone of the tibia, the cortical compartment was a 1 mm-long region centered at the tibial midshaft. Total cross sectional area (CSA, mm^2), medullary area (MA, mm^2) and cortical thickness (Ct.Th, mm) were assessed. Bone was segmented from soft tissue using the same threshold for all groups: 247 mg HA/cm^3 for trabecular and 245 mg HA/cm^3 for cortical bone.

Histology and Bone Histomorphometry

Static and dynamic histomorphometry was performed on methyl methacrylate-embedded tibiae as we have described (Shankar *et al.*, 2006). 20 mg/kg calcein was injected 7 days and 3 days prior to sacrifice (n=4-5 animals per group). Parameters in the tibial diaphysis and metaphysis were collected in a blinded fashion using a BH-2 digitizing morphometry system (Olympus, Center Valley, PA) and data were obtained by manual tracing (Osteometrics, Inc., Decatur, GA). Measurements of bone formation and resorption, including bone formation rate (BFR/BS), mineralizing surface (MS/BS), resorption rate (BRR/BS), and erosion surface (ES/BS) were made analogously to standard dynamic bone histomorphometry in unstained sections under UV illumination (Dempster *et al.*, 2013).

Similarly, two serial cross-sections of each tibia were obtained, the first of which was stained with von Kossa and tetrachrome, the second of which was stained with alkaline phosphatase (Shankar *et al.*, 2006). All histomorphometric examination was performed in a blinded, non-biased manner using a computerized semi-automated OsteoMeasure system (OsteoMetrics Inc.,

Atlanta, GA) as previously described (Shankar *et al.*, 2006). All measurements were confined to the secondary spongiosa and restricted to an area between 700 and 1500 um distal to the growth plate metaphyseal junction of the proximal tibia. A minimum of 25 fields in the proximal tibia were evaluated. Toluidine blue and Hoechst and Eosin--stained sections were assessed to determine total tissue area, total bone area, and total bone surface, and eroded surface. Tartrate-resistant acid phosphatase staining was used to determine osteoclast number and osteoclast surface. Within the same region of interest, alkaline phosphatase staining identified osteoblast surface, osteoblast number, and osteoblasts per bone area.

Western blotting

Cellular proteins were extracted from frozen bone samples as described previously (Chen *et al.*, 2008). NOX4 expression was detected using an antibody reactive to mouse NOX4 (Santa Cruz Biotechnologies, Inc., Santa Cruz, CA) followed by incubation with goat anti-rabbit secondary antibody conjugated with horseradish peroxidase (Santa Cruz Biotechnology). Total protein per sample was detected by Amido black staining (Boston Bioproducts, Ashland, MA).

RNA extraction and Reverse transcriptase (RT)-qPCR

Marrow-depleted femurs were ground and mRNA extracted in TRIzol reagent and Qiagen RNAplus Easy Kit (Qiagen, Hilden, Germany). cDNA was made using BioRad iScript reverse transcriptase (BioRad, Hercules, CA). Gene expression was analyzed using SYBR-Green on ABI 7500 real time PCR (American Bioanalytical, Natick, MA). Frozen lumbar vertebrae were crushed with a mortar and pestle and mRNA extracted in TRIzol reagent, followed by phase separation in 1-bromo-3-chloropropane (MBI) and isopropanol/ethanol washes. Gene expression was analyzed using Power SYBR-Green RNA-to-Ct 1-step kit (Applied Biosystems) on a Roche

LightCycler 480 thermal cycler (ThermoFisher Scientific, Waltham, MA). Results were calculated normalized to 18s ribosomal RNA.

Wnt array

Three RNA samples from each treatment group were randomly selected and applied to a primer array (Qiagen PAMM-043ZF-24) comprising 84 targets related to the canonical and non-canonical Wnt pathway. Results were normalized to an additional four housekeeping primers (*Actb, B2m, Gapdh, Gusb, Hsp90ab1*). Delta Ct values ($Ct_{target} - Ct_{housekeeping\ avg.}$) were analyzed for significant differences among groups by one-way ANOVA, and expression levels were evaluated as fold change vs housekeeping ($2^{(-deltaCt)}$) and fold change vs WT pair fed ($2^{(-delta*deltaCt)}$). The absence of genomic DNA contamination was confirmed by a genomic DNA control amplification threshold value greater than 35 cycles, according to manufacturer recommendations (Qiagen).

Cell Culture

Bone marrow was flushed from tibiae and femurs of 9-10 week old NOX4 -/-, p47phox -/-, and WT male mice by centrifugation passed through a 70 um filter as described (Chen *et al.*, 2010). Bone marrow cells were plated at 320,000 cells/cm^2 in parafilm-sealed flasks (Corning, Corning NY) in alpha minimal essential medium (aMEM, Gibco (Thermo Fisher), Grand Island, NY) supplemented with 10% fetal bovine serum and 1% penicillin/streptomycin (Gibco) as biologically independent replicates within six independent experiments. The medium was allowed to equilibrate to incubator conditions (37 deg, 5% CO_2) for at least four hours prior to plating and media was changed every 2 days (50% volume) (Chen *et al.*, 2010). L-ascorbate phosphate was added to the media following equilibration at a concentration of 50 υM in the

flask. Where indicated, ethanol was added to the media at a final concentration of 50 mM in the flask. On day 14, cultures were fixed and stained for alkaline phosphatase using an alkaline phosphatase detection kit according to the manufacturer's protocol (Sigma procedure #85) with Fast Blue or Fast Violet RR Salt (Sigma). Alkaline phosphatase colonies (AP+ CFU-F) were enumerated. Cultures were then counterstained with Gil's Hematoxylin and total colonies enumerated (Total CFU-F).

Statistical analysis

Except where noted, differences between genotypes and ethanol treatment, along with any interaction effects, were determined using two-way ANOVA followed by a Student-Newman-Keuls post-hoc test. All analyses were performed at alpha = 0.05 using SigmaPlot v. 11.0 or Microsoft Excel (2016) and significance ($p<0.05$) is reported as such. Summary statistics listed in the text are mean +/- SEM.

Results

The objective of this study was to test the overall hypothesis that NOX4 is instrumental in the *in vivo* suppression of bone formation by EtOH, where mice lacking NOX4 activity would retain osteoblast differentiation and activity, tissue mineralization, and bone structure regardless of EtOH consumption. Male, C57Bl/6J mice homozygous for ablation of exon 4 of the NOX4 gene (B6.129-NOX4^{Tm1Kkr}/J, Jackson Labs, Bar Harbor, ME) (Carnesecchi *et al.*, 2011) were investigated in comparison to wild type (WT) mice of the same age and sex (commencing at the post-pubertal age of 13 weeks when longitudinal growth had ceased). Following a 12-week exposure to either an EtOH liquid diet or calorically paired high fat diet, tibias were collected and analyzed for structural phenotype of the trabecular (metaphysis) compartment and cortical

midshaft (diaphysis) by micro-CT. Three-dimensional reconstructions of the trabecular bone region of interest are shown (Figure 1).

As expected, EtOH consumption produced a significant decrease in fractional bone volume (BV/TV) in WT mice (21.6 +/- 0.11% in WT PF vs. 16.1 +/- 0.45% in WT EtOH). However, and contrary to our hypothesis, NOX4 deletion did not protect bone in the trabecular (cancellous bone) compartment of mice consuming EtOH (18.7 +/- 1.1% in NOX4 -/- PF vs. 10.9 +/- 1.8% in NOX4-/- EtOH) (Figure 1A). Rather, NOX4 deletion exacerbated the EtOH effect (Figure 1B, $p = 0.014$ vs. WT EtOH). Trabecular number (Tb.N) decreased significantly only in ethanol-fed NOX4 -/- mice (5.34 +/- 0.06 per mm and 4.99 +/- 0.16 per mm for WT PF and EtOH, respectively; 5.21 +/- 0.11 per mm and 3.06 +/- 0.49 per mm for NOX4-/- PF and NOX4-/- EtOH, respectively) with a corresponding borderline statistically significant increase ($p = 0.08$ compared to NOX4 -/- pair-fed) in trabecular spacing (Tb.Sp) (0.177 +/- 0.0042 mm and 0.189 +/- 0.0083 mm for WT PF and WT EtOH, respectively; 0.178 +/- 0.0039 mm and 0.363 +/- 0.068 mm for NOX4-/- PF and NOX4 -/- EtOH, respectively). Together, these results suggest that NOX4 deletion increases the susceptibility of the trabecular compartment to EtOH's adverse effects on bone.

In contrast, the cortical compartment at the tibia midshaft of NOX4 -/- mice displayed a modest protection against the effect of EtOH treatment to decrease cortical bone parameters (Figure 1C, 1D). Despite a subtle but statistically significant decrease in cortical thickness in EtOH-fed WT mice ($p = 0.04$ vs. WT PF), there was no significant decrease in cortical thickness in EtOH-fed NOX4 -/- ($p = 0.167$ vs. NOX4-/- PF; 0.204 +/- 0.0041 mm and 0.190 +/- 0.0025 mm for WT PF and WT EtOH, respectively; 0.202 +/- 0.0064 mm and 0.193 +/- 0.0044 mm for NOX4-/- PF and NOX4-/- EtOH, respectively) (Fig 1D, Ct.Th). However, EtOH-fed NOX4 -/-

JPET Fast Forward. Published on April 13, 2018 as DOI: 10.1124/jpet.117.247262
This article has not been copyedited and formatted. The final version may differ from this version.

mice had smaller bones overall, as indicated by a significant decrease in bone area (0.336 +/- 0.0049 mm^2 and 0.328 +/- 0.0088 mm^2 for WT PF and WT EtOH, respectively; 0.326 +/- 0.0058 mm^2 and 0.294 +/- 0.014 mm^2 for NOX4-/- PF and NOX4-/- EtOH, respectively; $p = 0.043$ NOX4-/- PF vs. NOX4-/- EtOH), with genotype-driven decreases in total area (0.596 +/- 0.017 mm^2 and 0.607 +/- 0.023 mm^2 for WT PF and WT EtOH, respectively; 0.562 +/- 0.025 mm^2 and 0.517 +/- 0.037 mm^2, respectively; $p = 0.27$ NOX4-/- PF vs. NOX4-/- EtOH) and medullary area (0.343 +/- 0.014 mm^2 and 0.345 +/- 0.0060 mm^2 for WT PF and WT EtOH, respectively; 0.313 +/- 0.015 mm^2 and 0.318 +/- 0.021 mm^2 for NOX4-/- PF and NOX4-/- EtOH, respectively; $p = 0.69$ NOX4-/- PF vs. NOX4-/- EtOH) compared to WT controls (Figs 1D T.Ar, B.Ar, Med.Ar).

To determine whether the differences in bone volume were the result of diminished bone formation, mice were subcutaneously injected with calcein label 7 days and 3 days prior to sacrifice. Dynamic histomorphometry parameters of mineral apposition rate (MAR) and bone surface area-normalized bone formation rate (BFR/BS) were not significantly altered by genotype or ethanol treatment (Table 1). However significant decreases in bone area with NOX4 deletion (0.556 mm^2 for WT (PF and EtOH average), 0.415 mm^2 for NOX4 -/- (PF and EtOH average), $p < 0.05$ for genotype effect, two-way ANOVA) and significantly lower total volume-normalized bone WT volume (BV/TV) was observed in NOX4-/- EtOH-treated animals compared to WT pair fed animals (23.24% for WT pair fed, 17.01% for NOX-/- EtOH, $p<0.05$). NOX4 deletion significantly decreased the total number of osteoblasts (Table 2) compared to WT (93.0 ± 7.3 in WT, 58.2 ± 6.9 in NOX4 -/-; $p < 0.01$ for main genotype effect, two-way ANOVA). Among the mice treated with EtOH, NOX4 -/- mice had fewer osteoblasts compared to WT pair-fed mice (99.3 ± 10.7 in WT pair-fed, 48.2 ± 8.9 in NOX4 -/- EtOH, $p < 0.05$) and fewer osteoblasts compared to WT EtOH-fed mice with borderline significance (86.6 ± 12.3 in

WT pair-fed, p=0.06). When normalized to bone surface (Ob.S/BS), the genotype difference was no longer statistically significant. EtOH did not significantly decrease osteoblast number overall. However, total area-normalized osteoblast count (N.Ob/T.Ar) was significantly decreased by NOX4 deletion (Table 2, 160.3 ± 9.2 Ob/mm^2 in WT, 104.5 ± 11.8 Ob/mm^2 in NOX4 -/-; $p < 0.01$ for main genotype effect, two-way ANOVA), and NOX4 -/- animals treated with ethanol had fewer total area-normalized osteoblast count compared to the other three groups (174.0 ± 11.5 Ob/mm^2 Ob/mm^2 in WT Pair Fed, 146.6 ± 12.0 Ob/mm^2 in WT EtOH, 129.9 ± 14.0 in NOX4 -/- Pair Fed, 79.05 ± 10.5 Ob/mm^2 in NOX4-/- EtOH, $p<0.05$, two-way ANOVA). The data suggest an exacerbation of the suppressive effect of EtOH on osteoblast differentiation, and a decrease in total osteoblast activity, in the absence of NOX4. No significant differences were observed among treatments or genotypes for measures of osteoclast prevalence or activity (Supplemental Table 1).

To identify intracellular mechanisms contributing to the observed phenotypes, total RNA was extracted from femur cortices and vertebral bone, and gene expression (relative to 18s rRNA) was determined by RT-qPCR (Figure 2). As was observed via micro-CT, ethanol appeared to have a compartment-specific effect. Vertebral bone, which is largely trabecular, but not the femur cortical midshaft, appeared to be sensitive to the anti-osteogenic effect of ethanol regardless of NOX4 expression. In cortical bone, ethanol-fed WT mice displayed significantly reduced expression of the osteogenic genes osteocalcin (*Bglap*) (Fig 2A) and collagen 1a1 (*Col1a1*) (Fig 2B) compared to WT pair-fed controls ($p = 0.007$ and 0.002, respectively), whereas ethanol had no effect on the expression of these genes in NOX4 -/- mice ($p = 0.612$ and 0.997, for *Bglap* and *Col1a1*, respectively). Ethanol did not have a NOX4-dependent effect in vertebral bone: overall, ethanol suppressed alkaline phosphatase expression with borderline

statistical significance (Fig 2C, p=0.08 for main effect of ethanol, 2-way ANOVA) and suppressed collagen 1a1 expression (Fig 2D, p = 0.05 for main effect of ethanol, 2-way ANOVA).

NADPH oxidase 2 (NOX2) and RANKL expression are related to ethanol-induced bone resorption (Mercer *et al.*, 2014). In cortical samples from WT mice, EtOH upregulated mRNA expression of NOX2 compared to pair-fed mice (Fig 2E) ($p < 0.003$). This was accompanied by significant increases in NOX2 expression in both pair-fed and EtOH-fed NOX4-/- mice compared to WT pair-fed, although there was no effect of EtOH on NOX4-/- mice. As expected, EtOH significantly upregulated the expression of *Rankl* in both WT and NOX4 -/- mice ($p < 0.0001$ for main effect of EtOH, two-way ANOVA) (Fig 2F). Notably, NOX4 -/- animals showed higher expression of *Rankl* compared to WT ($p = 0.012$ for main effect of genotype, two-way ANOVA), with NOX4 -/- EtOH mice showing a potentiated increase in *Rankl* expression ($p < 0.001$ compared to WT EtOH). Consistent with previous data showing upregulation of NOX4 mRNA and protein in EtOH-treated rats (Chen *et al.*, 2011), NOX4 protein expression increased in WT, EtOH-fed mice (Figure 3).

A critical driver of osteoblast differentiation is the canonical Wnt pathway (Duan and Bonewald, 2016). To determine whether EtOH affects aspects of this pathway *in vivo*, vertebral mRNA (n = 3 for each group) was applied to a Qiagen Wnt pathway array (Qiagen) that assays 84 separate Wnt targets. Expression levels of each gene were normalized to expression levels of internal housekeeping genes (*Actb, B2m, Gapdh, Gusb, Hsp90ab1*) (Fig 4A), and target gene up- or down-regulation was determined relative to pair-fed WT samples (Fig 4B). There was no significant difference among the proportions of up- and down-regulated targets in the three groups relative to pair-fed WT (chi square, p=0.446). However, one-way ANOVA of the

housekeeping-adjusted values for all four groups identified statistically significant expression variation for 11 gene targets: three Wnt ligand molecules (*Wnt3, Wnt4, Wnt6*), two Frizzled receptor genes (*Fzd5, Fzd8*), beta catenin (*Ctnnb1*), four genes related to beta-catenin accumulation (*Cnsk2a1*), degradation (*Gsk3b, Fbxw4*) and DNA binding (*Tcfl7*), and Wnt signaling target gene *Ccnd2*.

To confirm these results, trabecular mRNA expression was evaluated for individual targets using RT-qPCR and results were analyzed by two-way ANOVA (Figure 5). As a main effect, ethanol was found to significantly suppress expression of the gene encoding Wnt target cyclin D2 (*Ccnd2*) and a suppressive effect approached statistical significance for Frizzled receptor-8 (*Fzd8*, main effect of ethanol $p = 0.10$, 2-way ANOVA). Expression of beta catenin (*Cttnb1*) mRNA was non-significantly upregulated by ethanol in both groups ($p = 0.11$). Deletion of NOX4 produced a borderline significant main effect in two-way ANOVA seen in *Ccnd2* expression (main effect of genotype $p = 0.07$, 2-way ANOVA) and borderline significant suppression of *Wnt6* (main effect of genotype $p = 0.06$). No significant effects were found for expression of *Fbxw4* or *Fzd8*; *Wnt3* and *Wnt4* mRNA did not amplify sufficiently in RT-qPCR for the purpose of analysis. Thus, in contrast to the cortical data where the effects of EtOH and NOX4 deletion appear to interact, trabecular effects of EtOH and NOX4 appeared to be independent.

To further elucidate the effect of EtOH on osteoblast differentiation in the context of NOX4 deletion, osteoblasts were differentiated from bone marrow mesenchymal stromal cell (BM-MSC) primary cultures. BM-MSCs from male and female, 9-10 week old mice were flushed from the femur and tibia bone marrow and incubated in sealed flasks for 14 days in the presence of 50 uM l-ascorbate phosphate alone or with 50 μM l-ascorbate plus 50mM EtOH. At

the end of the treatment period, cell cultures were assayed for fibroblast colony forming units (CFU-Fs) by Gil's hematoxylin and for alkaline phosphatase as an indicator of osteoblast colony forming units (AP+ CFU-Fs) (Figure 6). BM-MSCs derived from NOX4 -/- mice consistently developed fewer CFU-Fs compared to BM-MSCs derived from WT mice (6.80 +/- 0.472 colonies vs. 18.01 +/- 1.36 colonies per 1 million cells plated, respectively; main effect of genotype $p < 0.0001$, two-way ANOVA). In contrast, EtOH had no significant effect on the number of CFU-Fs within each genotype (Fig 6A). However, 50 mM EtOH treatment revealed a differential effect with respect to AP+ CFU-OBs. Normalized to hematoxylin-positive colonies, AP+ CFU-F counts were suppressed by EtOH in WT cultures (75.6% in untreated, 52.8% in EtOH-treated cultures), whereas EtOH treatment was non-significantly increased in AP+ CFU-Fs in NOX4 -/- cultures (66.9% in untreated, 76.1% in EtOH-treated cultures, p-value for interaction = 0.006, two-way ANOVA) (Fig 6B, 6C). Colonies derived from bone marrow harvested from $p47^{phox}$ -/- mice (B6N.129S2-*Ncf1*^{tm1Shl}/J, Jackson Labs), of the same age and sex, lacking $p47^{phox}$ (an essential signaling component of NOX2) were not protected against EtOH's suppression of alkaline phosphatase ($p < 0.001$ vs $p47^{phox}$ -/- without EtOH) (Fig 6D). Together, these data suggest an overall support of osteoblast colony formation, but a sensitivity to the EtOH-mediated suppression of osteoblast maturation, in WT BM-MSCs compared to those lacking NOX4.

Discussion

Chronic alcohol consumption can lead to a variety of health issues, including increased risk of osteopenia and bone fracture (González-Reimers *et al.*, 2011, Santori *et al.*, 2008). EtOH increases bone resorption and suppresses osteogenesis in part by increasing oxidative stress in osteoblasts (Chen *et al.*, 2010). This mechanism appears to be dependent on the metabolism of

EtOH by alcohol dehydrogenase (ADH) (Mercer *et al.*, 2014). EtOH metabolism by ADH increases the cellular pool of NADPH. In response, elevated activity of the NOX enzymes, particularly NOX4 and NOX2, produce excess superoxide and hydrogen peroxide via the action of superoxide dismutase (Schroder, 2015). Hydrogen peroxide can prevent murine osteoblast differentiation and expression of alkaline phosphatase (Atashi *et al.*, 2015). The finding that antioxidant administration can robustly prevent EtOH's suppression of bone homeostasis confirms the involvement of ROS in EtOH's mechanism of action (Shankar *et al.*, 2008; Chen *et al.*, 2010; Alund *et al.*, 2017). However, the degrees to which different NOX enzymes contribute to EtOH's alterations of bone phenotype are largely unresolved.

NOX4 and NOX2 drive oxidative stress in bone cells in a complimentary manner, as pan-inhibition of NOX2 and NOX4 by DPI reduces hydrogen peroxide generation in the mouse ST2 mesenchymal cell line (Mercer *et al.*, 2014). We previously demonstrated that functional NOX2 deletion prevents EtOH-mediated increases in bone resorption, but does not prevent the suppression of bone formation: despite loss of functional NOX2, EtOH significantly downregulated serum osteocalcin, indicating a suppression of anabolic activity in bone (Mercer *et al.*, 2014). These results implied a central role of the predominately-expressed NOX4 in EtOH's impairment of bone homeostasis. Hence, this study was designed to determine the contribution of NOX4 activity to the suppression of bone formation with chronic EtOH consumption utilizing a global NOX4 knockout mouse model.

NOX4 deletion has previously been suggested to support bone mass. Specifically, NOX4 -/- mice were reported to have a ~30% increase in trabecular bone volume despite no significant change in histological osteoblast parameters (Goettsch *et al.*, 2013). Contrary to those observations, the micro-CT results presented herein (Figure 1A and 1B) indicate no change in

trabecular bone mass with NOX4 deletion alone, but an exacerbated effect of EtOH to reduce trabecular bone mass in NOX4-/- mice. Differences between these studies may include the use of male mice and the age at start of treatment (13 weeks; the age and sex of intact mice used by Goettsch *et al.* is not noted) as well as the genetics of NOX4 deletion. Whereas Goettsch *et al.* deleted NOX4 via ablation of exons 1 and 2, the mice in the current study had exon 4 deleted (Carnesecchi *et al.*, 2011). The latter method prevented amplification of mRNA targeting exon 4 (Supplemental Figure 1) and was shown by others to abolish NOX4 expression in the spleen, kidney and lung (Carnesecchi *et al.*, 2011). Further investigation into alternate mechanisms associated with loss of NOX4, including compensatory NOX2 activity (suggested by increases in NOX2 mRNA (Fig 2E)) or NOX1 (Wittrant *et al.* 2009) expression, are ongoing in our laboratory. Loss of NOX4 activity does not necessarily limit oxidative stress with EtOH, which may also be associated with increases in mitochondrial derived ROS. Addition of a NOX4-specific inhibitor, plumbagin, did not significantly prevent the accumulation of hydrogen peroxide in cultured, EtOH-treated ST2 cells (Mercer *et al.*, 2014).

Micro-CT data indicated that cortical bone in NOX4 -/- mice was less susceptible to bone loss following EtOH exposure. These mice had smaller tibias overall (i.e. lower total cross sectional area) but maintained cortical bone thickness compared to NOX4-/- pair-fed controls, results substantiated by RT-qPCR data of cortical osteocalcin and collagen 1a1 mRNA expression. Only EtOH-fed WT mice showed a significant decrease in cortical thickness. Given the significant decrease in trabecular bone loss in EtOH-fed WT mice, suggesting acceleration of endosteal bone turnover, medullary area was expected to significantly increase in parallel with significant cortical thinning. However, it appeared that the slight increase in total area with EtOH in WT mice, along with measurement variability, may have obscured this observation. In sum,

NOX4 deletion appears to be protective of EtOH's reduction in cortical thickness but susceptible to EtOH's reduction in overall bone and total area.

RT-qPCR analyses of specific mRNA targets in trabecular bone suggest a compartment-specific effect of NOX4 and EtOH: in contrast to cortical bone, vertebral bone (which is predominately trabecular) had suppressed collagen 1a1 expression with EtOH regardless of genotype (Figure 2D). Differences in the regulation of bone mass in the cortical vs. trabecular compartments have been reported (e.g. Alund *et al.*, 2016, 2017). For example, Alund *et al*. (2017) showed that dietary antioxidant co-administration protected against trabecular bone loss but not cortical bone loss with EtOH. Similarly, transgenic mice overexpressing human catalase were protected against EtOH-induced loss of trabecular bone, though cortical bone mineral density was significantly reduced (Alund *et al.*, 2016). One notable difference between the two compartments is the greater osteocyte population in the cortex, which contribute to bone remodeling by promoting osteoclast differentiation through RANKL expression (Sims and Martin, 2014) and by secreting mineralizing factors such as DMP1 and PHEX (Bonewald, 2011). Moreover, NOX4 plays a direct role in osteoclast differentiation downstream of RANKL/RANK binding (Yang *et al.*, 2004), therefore global deletion of NOX4 may supersede any osteoclastic effect of increased RANKL mRNA expression in cortical bone osteocytes (Fig 2F). This idea is supported by increases in NOX2 mRNA expression (Fig. 2E) previously shown to be associated with RANKL expression (Mercer *et al.*, 2014). Future studies using Cre-Lox models that delete NOX4 or NOX2 specifically in early osteoblasts or mature osteocytes, or by site-specific deletion driven by the long bone-specific Prx-1 promoter (Logan *et al.*, 2002), will help elucidate the apparent compartmental or site-specific effects related to NOX4.

The Wnt pathway, which supports bone formation, is suppressed by oxidative stress (Almeida *et al.*, 2007a). Chen *et al*. (2010) showed that the Wnt pathway is a sensitive target of EtOH's effect on bone through an oxidative stress-related mechanism. In this context, Wnt pathway targets in samples of vertebral bone were probed to confirm whether the suppressive effect of EtOH was NOX4-dependent. In contrast to Chen et al. (2010), where administration of the dietary antioxidant N-acetylcysteine eliminated EtOH's suppression of Wnt-related genes, NOX4 deletion (which might also be expected to blunt the production of ROS) did not protect against a suppression of the end target gene *Ccnd2*. In general, EtOH suppressed various steps along the canonical pathway. Thus, although NOX4 is a significant source of oxidative stress, and ROS interfere with canonical Wnt signaling (Chen *et al.*, 2010, Almeida *et al.*, 2007a), there appear to be other EtOH-induced oxidative stress mechanisms (e.g. mitochondrial ROS) that contribute to a ROS-related reduction in Wnt signaling independent of NOX4.

Epithelial models employing angiotensin II have provided evidence of cross-talk between NOX-induced and mitochondrial ROS (Dikalov, 2011). Deleting $p22^{phox}$ – the common subunit among NOX isoforms – blocks mitochondrial ROS increases by angiotensin II (Doughan *et al.*, 2008). Conversely, blocking mitochondrial superoxide dismutase (causing an increase in mitochondrial superoxide) elevates NOX activity; together, these mechanisms amplify ROS (Dikalova *et al.*, 2010). NOX isoforms also show interdependence. Among NADPH oxidases, hydrogen peroxide increases NOX2 superoxide radical formation in fibroblasts (Li *et al.*, 2001). Future studies will resolve the complex picture describing ROS generation as a function of multiple intracellular sources using mitochondria-specific inhibitors (e.g. mitoTEMPO) and cell type- and isoform-specific NOX knockout models.

An important finding in this study is that NOX4 deletion results in a lower capacity to form fibroblast colonies (CFU-F). It also bears noting that these *in vitro* results paralleled the static histomorphometry analyses, showing a smaller population of osteoblasts that, on a per-area basis, produced less bone in response to EtOH. It has been suggested that an optimal level of reactive oxygen species are necessary for appropriate osteoblast differentiation (Schroder, 2015). Deletion of NOX4 may present a phenotype whereby MSCs have a diminished capacity for self-renewal or for the early stages of differentiation. As a result, the effects of NOX4 deletion and EtOH on bone formation, particularly in the MSC-rich trabecular compartment, are additive.

Bone loss results from a severe imbalance of resorption and formation. NOX4 deletion protects bone from EtOH-induced mineral loss that is observable in the osteocyte-dominated cortical compartment. Although it appears a compensatory upregulation of NOX2 under NOX4 deletion is concurrent with an upregulation of RANKL in cortical bone, exactly how this effect may interact with a loss of NOX4-dependent osteoclast differentiation is not yet known. Non-bone sources of RANKL, such as the EtOH-injured liver (Araujo Junior *et al.* 2016), may influence this dynamic. More observable in the NOX4 -/- model was a suppression of functional osteoblast differentiation that would target the osteoblast-rich trabecular compartment, generating a lower baseline level of trabecular bone. Further studies will elucidate, via cell-specific knockouts, the NOX isoform-dependent steps in osteoblast differentiation and target the intracellular communication between osteoblasts and osteoclasts that functionally determines the balance of bone turnover in the presence of EtOH.

Authorship contributions

Participated in research design: Ronis, Alund, Pulliam, Watt, Mercer

Conducted experiments: Alund, Pulliam, Watt

Conducted analyses: Chen, Suva

Performed data analysis: Alund, Watt, Chen

Wrote or contributed to the writing of the manuscript: Watt, Alund, Ronis, Suva

References

Almeida M, Han L, Martin-Millan M, O'Brien CA, and Manolagas SC (2007a) Oxidative stress antagonizes Wnt signaling in osteoblast precursors by diverting beta-catenin from T cell factor- to forkhead box O-mediated transcription. *J Biol Chem* **282**:27298–305.

Almeida M, Han L, Martin-Millan M, Plotkin LI, Stewart SA, Roberson PK, Kousteni S, O'Brien CA, Bellido T, Parfitt AM, Weinstein RS, Jilka RL, and Manolagas SC (2007b) Skeletal involution by age-associated oxidative stress and its acceleration by loss of sex steroids. *J Biol Chem* **282**:27285–97.

Alund AW, Mercer KE, Suva LJ, Pulliam CF, Chen J-R, Badger TM, Van Remmen H, and Ronis MJJ (2016) Reactive oxygen species differentially regulate bone turnover in an age-specific manner in catalase transgenic female mice. *J Pharmacol Exp Ther* **358**:50–60.

Alund AW, Mercer KE, Pulliam CF, Suva LJ, Chen J-R, Badger TM, and Ronis MJJ (2017) Partial protection by dietary antioxidants against ethanol-induced osteopenia and changes in bone borphology in female mice. *Alcohol Clin Exp Res* **41**:46–56.

Ambe K, Watanabe H, Takahashi S, and Nakagawa T (2014) Immunohistochemical localization of NOX1, NOX4 and Mn-SOD in mouse femur during endochondral ossification. *Tissue Cell* **46**:433–438.

Araujo Junior RF, Garcia VB, Leitao RF, Brito GA, Miguel Ede C, Guedes PM, de Araujo AA (2016) Carvedilol improves inflammatory response, oxidative stress and fibrosis in the alcohol-induced liver injury in rats by regulating kuppfer cells and hepatic stellate cells. *PLoS One* **11(2)**:e0148868.

Atashi F, Modarressi A, and Pepper MS (2015) The role of reactive oxygen species in mesenchymal stem cell adipogenic and osteogenic differentiation: a review. *Stem Cells Dev* **24**:1150–63.

Bai XC, Lu D, Liu AL, Zhang ZM, Li XM, Zou ZP, Zeng W Sen, Cheng BL, and Luo SQ (2005) Reactive oxygen species stimulates receptor activator of NF-kB ligand expression in osteoblast. *J Biol Chem* **280**:17497–17506.

Bedard K, and Krause K-H (2007) The NOX family of ROS-generating NADPH oxidases: physiology and pathophysiology. *Physiol Rev* **87**:245–313.

Bonewald LF (2011) The amazing osteocyte. *J Bone Miner Res* **26**:229–238.

Bouxsein ML, Boyd SK, Christiansen B a., Guldberg RE, Jepsen KJ, and Müller R (2010) Guidelines for assessment of bone microstructure in rodents using micro-computed tomography. *J Bone Miner Res* **25**:1468–86.

Brandes RP, Weissmann N, and Schröder K (2014) NOX family NADPH oxidases: Molecular mechanisms of activation. *Free Radic Biol Med* **76**:208–226.

Callaci JJ, Himes R, Lauing K, Wezeman FH, Brownson K (2009) Binge alcohol-induced bone damage is accompanied by differential expression of bone remodeling-related genes in rat vertebral bone. *Calcif Tissue Int* **84**:474-484.

Carnesecchi S, Deffert C, Donati Y, Basset O, Hinz B, Preynat-Seauve O, Guichard C, Arbiser JL, Banfi B, Pache J-C, Barazzone-Argiroffo C, and Krause K-H (2011) A key role for NOX4 in epithelial cell death during development of lung fibrosis. *Antioxid Redox Signal* **15**:607–619.

Chen J-R, Haley RL, Hidestrand M, Shankar K, Liu X, Lumpkin CK, Simpson PM, Badger TM, and Ronis MJJ (2006) Estradiol protects against ethanol-induced bone loss by inhibiting up-regulation of receptor activator of nuclear factor-κB ligand in osteoblasts. *J Pharmacol Exp Ther* **319**:1182–1190.

Chen J, Shankar K, Nagarajan S, Badger TM, and Ronis MJJ (2008) Protective effects of estradiol on ethanol-induced bone loss involve inhibition of reactive oxygen species generation in osteoblasts and downstream activation of the extracellular signal-regulated kinase / signal transducer and activator of transcription 3/receptor activator of nuclear factor-kB ligand signaling cascade. *J Pharmacol Exp Ther* **324**:50–59.

Chen JR, Lazarenko OP, Haley RL, Blackburn ML, Badger TM, and Ronis MJ (2009) Ethanol impairs estrogen receptor signaling resulting in accelerated activation of senescence pathways, whereas estradiol attenuates the effects of ethanol in osteoblasts. *J Bone Miner Res* **24**:221–230.

Chen JR, Lazarenko OP, Shankar K, Blackburn ML, Badger TM, and Ronis MJ (2010) A role for ethanol-induced oxidative stress in controlling lineage commitment of mesenchymal stromal cells through inhibition of Wnt/β-catenin signaling. *J Bone Miner Res* **25**:1117–1127.

Chen J, Lazarenko OP, Shankar K, Blackburn ML, Lumpkin CK, Badger TM, and Ronis MJJ (2011) Inhibition of NADPH oxidases prevents chronic ethanol-induced bone loss in female rats. *J Pharmacol Exp Ther* **336**:734–742.

Dallas SL, and Bonewald LF (2010) Dynamics of the transition from osteoblast to osteocyte. *Ann N Y Acad Sci* **1192**:437–443.

Dempster DW, Compston JE, Drezner MK, Glorieux FH, Kanis JA, Malluche H, Meunier PJ, Ott SM, Recker RR, Parfitt AM (2013) Standardized nomenclature, symbols, and units for bone

histomorphometry: a 2012 update of the report of the ASBMR Histomorphometry Nomenclature Committee. *J Bone Miner Res* **28**: 2-17.

Dikalov S (2011) Cross talk between mitochondria and NADPH oxidases. *Free Radic Biol Med* **51**:1289–1301.

Dikalova AE, Bikineyeva AT, Budzyn K, Nazarewicz RR, McCann L, Lewis W, Harrison DG, and Dikalov SI (2010) Therapeutic targeting of mitochondrial superoxide in hypertension. *Circ Res* **107**:106–116.

Doughan AK, Harrison DG, and Dikalov SI (2008) Molecular mechanisms of angiotensin II-mediated mitochondrial dysfunction: Linking mitochondrial oxidative damage and vascular endothelial dysfunction. *Circ Res* **102**:488–496.

Duan P, and Bonewald LF (2016) The role of the wnt/β-catenin signaling pathway in formation and maintenance of bone and teeth. *Int J Biochem Cell Biol* **77**:23–29, Elsevier Ltd.

Gaddini GW, Turner RT, Grant KA, and Iwaniec UT (2016) Alcohol: A Simple Nutrient with Complex Actions on Bone in the Adult Skeleton. *Alcohol Clin Exp Res* **40**:657–671.

Goettsch C, Babelova A, Trummer O, Erben RG, Rauner M, Rammelt S, Weissmann N, Weinberger V, Benkhoff S, Kampschulte M, Obermayer-Pietsch B, Hofbauer LC, Brandes RP, and Schroder K (2013) NADPH oxidase 4 limits bone mass by promoting osteoclastogenesis. *J Clin Invest* **123**:4731–4738.

González-Reimers E, Alvisa-Negrín J, Santolaria-Fernández F, Ros-Vilamajó R, Martín-González MC, Hernández-Betancor I, García-Valdecasas-Campelo E, and González-Díaz A (2011) Prognosis of osteopenia in chronic alcoholics. *Alcohol* **45**:227–238.

Komori T, Yagi H, Nomura S, Yamaguchi A, Sasaki K, Deguchi K, Shimizu Y, Bronson RT, Gao YH, Inada M, Sato M, Okamoto R, Kitamura Y, Yoshiki S, and Kishimoto T (1997) Targeted disruption of Cbfa1 results in a complete lack of bone formation owing to maturational arrest of osteoblasts. *Cell* **89**:755–64.

Li WG, Miller FJ, Zhang HJ, Spitz DR, Oberley LW, and Weintraub NL (2001) H2O2-induced $O2^-$ production by a non-phagocytic NAD(P)H oxidase causes oxidant injury. *J Biol Chem* **276**:29251–29256.

Long F (2011) Building strong bones: molecular regulation of the osteoblast lineage. *Nat Rev Mol Cell Biol* **13**:27–38, Nature Publishing Group.

Logan M, Martin JF, Nagy A, Lobe C, Olson EN, Tabin CJ (2002) Expression of a Cre recombinase in the developing mouse limb bud driven by a Prx1 enhancer. *Genesis* **33**: 77-80.

Martin TJ, and Seeman E (2008) Bone remodeling: its local regulation and the emergence of bone fragility. *Best Pract Res Clin Endocrinol Metab* **22**:701–722, Elsevier Ltd.

Mercer KE, Sims CR, Yang CS, Wynne RA, Moutos C, Hogue WR, Lumpkin CK, Suva LJ, Chen J-R, Badger TM, and Ronis MJJ (2014) Loss of functional NADPH oxidase 2 protects against alcohol-induced bone resorption in female p47phox-/- mice. *Alcohol Clin Exp Res* **38**:672–82.

Nyquist F, Ljunghall S, Berglund M, and Obrant K (1996) Biochemical markers of bone metabolism after short and long time ethanol withdrawal in alcoholics. *Bone* **19**:51–54.

Orwoll ES (2003) Toward an Expanded Understanding of the Role of the Periosteum in Skeletal Health. *J Bone Miner Res* **18**:949–954.

Poole KES, and Compston JE (2006) Osteoporosis and its management. *BMJ* **333**:1251–6.

Rzonca SO, Suva LJ, Gaddy D, Montague DC, and Lecka-Czernik B (2004) Bone is a target for the antidiabetic compound rosiglitazone. *Endocrinology* **145**:401–6.

Santori C, Ceccanti M, Diacinti D, Attilia ML, Toppo L, D'Erasmo E, Romagnoli E, Mascia ML, Cipriani C, Prastaro A, Carnevale V, and Minisola S (2008) Skeletal turnover, bone mineral density, and fractures in male chronic abusers of alcohol. *J Endocrinol Invest* **31**:321–326.

Schroder K (2015) NADPH oxidases in bone homeostasis and osteoporosis. *Cell Mol Life Sci* **72**:25–38.

Shankar K, Hidestrand M, Haley R, Skinner RA, Hogue W, Jo CH, Simpson P, Lumpkin CK, Aronson J, Badger TM, and Ronis MJJ (2006) Different molecular mechanisms underlie ethanol-induced bone loss in cycling and pregnant rats. *Endocrinology* **147**:166–178.

Shankar K, Hidestrand M, Liu X, Chen JR, Haley R, Perrien DS, Skinner RA, Lumpkin CK, Badger TM, and Ronis MJJ (2008) Chronic ethanol consumption inhibits postlactational anabolic bone rebuilding in female rats. *J Bone Miner Res* **23**:338–49.

Sims NA, and Martin TJ (2014) Coupling the activities of bone formation and resorption: a multitude of signals within the basic multicellular unit. *Bonekey Rep* **3**:1–10.

Suva LJ, Hartman E, Dilley JD, Russell S, Akel NS, Skinner RA, Hogue WR, Budde U, Varughese KI, Kanaji T, and Ware J (2008) Platelet Dysfunction and a High Bone Mass Phenotype in a Murine Model of Platelet-Type von Willebrand Disease. *Am J Pathol* **172**:430–439,

Wittrant Y, Gorin Y, Mohan S, Wagner B, Abboud-Werner SL (2009) Colony-stimulating factor-1 (CSF-1) directly inhibits receptor activator of nuclear factor-kappaB ligand (RANKL) expression by osteoblasts. *Endocrinology* **150**:4977-4988.

Yang S, Zhang Y, Ries W, and Key L (2004) Expression of NOX4 in osteoclasts. *J Cell Biochem* **92**:238–248.

Yang CS, Mercer KE, Alund AW, Suva LJ, Badger TM, Ronis MJ (2014) Genistein supplementation increases bone turnover but does not prevent alcohol-induced bone loss in male mice. *Exp Biol Med (Maywood)* **239**:1380-1389.

Footnotes

Footnote to title:

This work was supported in part by the National Institute on Alcohol Abuse and Alcoholism [R37 AA018282] (MJJR), National Institute of General Medical Sciences [T32 GM106999-01] "Systems Pharmacology & Toxicology" Training Program (University of Arkansas for Medical Sciences, UAMS) and UAMS CUMG Funds.

Figure Legends

Figure 1. NOX4 -/- mice have reduced trabecular bone volume but sustained cortical bone mass with EtOH. (A) Micro-computed tomography (micro-CT) images of the trabecular compartment (12 um resolution). (B) Micro-CT-evaluated trabecular bone parameters: fractional bone volume (BV/TV); trabecular number (Tb.N); trabecular spacing (Tb.Sp). N for each group: WT PF: 3; WT EtOH 4; NOX4 -/- PF: 3; NOX4 -/- EtOH: 5. (C) Micro-CT images of cortical compartment (12 um resolution). (D) Micro-CT-evaluated cortical bone parameters: cortical thickness (Ct.Th); total area (T.Ar); bone area (B.Ar); medullary area (M.Ar). N for each group: WT PF: 4; WT EtOH 5; NOX4 -/- PF: 4; NOX4 -/- EtOH: 5. Statistical significance was determined with two-way analysis of variance; values with different letter superscripts are statistically different from each other ($p < 0.05$, Student-Newman-Keuls post hoc test; a*: p=0.08 for comparison of mean to NOX4 -/- pair fed).

Figure 2. NOX4 deletion is protective of EtOH-induced anti-osteogenic effects in cortical, but not trabecular bone. (A) Cortical bone-derived osteocalcin (*Bglap*); (B) cortical bone-derived collagen 1a1 (*Col1a1*); (C) vertebral bone-derived alkaline phosphatase (*Alpl*); (D) vertebral bone-derived collagen 1a1 (*Col1a1*); (E) cortical bone-derived NADPH oxidase 2 (*Nox2*); (F) cortical bone-derived RANKL (*Rankl*). n = 3-5 for each group. Statistical significance was determined with two-way analysis of variance; values with different letter superscripts are statistically different from each other ($p < 0.05$, Student-Newman-Keuls post hoc test).

Figure 3. Ethanol increases expression of NOX4 protein in WT mice. Representative samples (n=3 pair fed and 3 EtOH) of total protein from WT mice isolated following aspiration of bone marrow. Top: anti-NOX4 antibody (Santa Cruz Biotechnologies). Amido black staining of total

protein. Bottom: densitometric quantification of Western immunoblots. * $p < 0.05$, Student's unpaired t-test.

Figure 4. Distribution of Wnt pathway array gene expression among treatment groups. (A) Fold change in gene expression relative to housekeeping genes (*Actb, B2m, Gapdh, Gusb, Hsp90ab1*). (B) Relative changes in gene expression (upregulated or downregulated) in groups relative to WT pair fed. Open square: upregulated; closed circle: downregulated. Distributions of relative gene expression not statistically significant ($p > 0.05$; chi-square). n = 3 from each group.

Figure 5. EtOH significantly downregulates targets of the Wnt pathway in vertebral bone. (A) Cyclin D2 (*Ccnd2*); (B) Frizzled-5 precursor (*Fzd5*); (C) Frizzled-8 precursor (*Fzd8*); (D) Beta-catenin (*Cttnb1*); (E) Wnt-6 (*Wnt6*); (F) F-box/WD repeat-containing protein 4 (*Fbxw4*). Results analyzed by two-way ANOVA, significant main effects highlighted and bolded ($p < 0.05$); borderline significant effects ($p \leq 0.10$ in bold only). n for each group: WT pair fed: 4; WT EtOH: 5; NOX4 -/- pair fed: 5; NOX4 -/- EtOH: 6.

Figure 6. NOX4 -/- bone marrow mesenchymal stromal cells (BM-MSCs) from 9-10 week old male and female mice develop fewer fibroblast colonies but are protected against EtOH's suppression of alkaline phosphatase. (A) Count of hematoxylin-positive fibroblast colonies (CFU-F) per million cells plated. (B) Percent of hematoxylin-positive colonies that stained positive for alkaline phosphatase. (C) Representative images of WT (top) and NOX4-/- (bottom) cultures treated with or without ethanol, following staining for alkaline phosphatase using Fast Blue (WT) or Fast Violet (NOX4 -/-) salt. Arrow: representative punctate AP+ CFU-F. (D) Percent of hematoxylin-positive colonies that stained positive for alkaline phosphatase (p47: cultures extracted from $p47^{phox}$ -/- animals lacking functional NOX2). Statistical significance was

determined with two-way analysis of variance; values with different letter superscripts are statistically different from each other ($p < 0.05$, Tukey's multiple comparisons analysis). n for each group: WT 0 mM EtOH: 15; WT 50 mM EtOH: 12; NOX4-/- 0 mM: 7; NOX4 -/- 50 mM: 7.

JPET Fast Forward. Published on April 13, 2018 as DOI: 10.1124/jpet.117.247262
This article has not been copyedited and formatted. The final version may differ from this version.

	WT Pair Fed (n = 4)	WT EtOH (n = 5)	NOX4 -/- Pair Fed (n = 5)	NOX4 -/- EtOH (n = 5)
T.Ar (mm^2)	2.23 ± 0.15	2.38 ± 0.12	2.24 ± 0.25	2.21 ± 0.20
B.Ar (mm^2)	0.51 ± 0.004 † a	0.60 ± 0.08 † a	0.41 ± 0.02 b	0.42 ± 0.04 b
BV/TV (%)	23.23 ± 1.46 †,‡ a	20.49 ± 1.31 †,‡ a,b	20.89 ± 1.36 a,b	17.01 ± 1.25 b
MAR (μm/d)	2.78 ± 0.25	2.93 ± 0.33	3.16 ± 0.31	3.41 ± 0.21
BFR/BS ($\mu m^3/\mu m^2/d$)	0.72 ± 0.21	0.62 ± 0.17	0.78 ± 0.12	0.62 ± 0.18

Table 1. Dynamic histomorphometry parameters. Abbreviations: T.Ar: total area; B.Ar: bone area; BV/TV: fractional bone volume; MAR: mineral apposition rate; BFR/BS: bone surface-normalized bone formation rate. Means +/- SEM. † significant main effect of genotype (WT vs. NOX4 -/-); ‡ significant main effect of EtOH (PF vs. EtOH) ($p < 0.05$, two-way ANOVA). Values with different letter superscripts are statistically different from each other ($p < 0.05$, two-way ANOVA, Student-Newman-Keuls post hoc test).

JPET Fast Forward. Published on April 13, 2018 as DOI: 10.1124/jpet.117.247262
This article has not been copyedited and formatted. The final version may differ from this version.

	WT Pair Fed (n = 4)	WT EtOH (n = 5)	NOX4 -/- Pair Fed (n = 5)	NOX4 -/- EtOH (n = 5)
T.Ar (mm^2)	0.569 ± 0.044	0.595 ± 0.070	0.525 ± 0.0001	0.595 ± 0.043
B.Ar (mm^2)	0.071 ± 0.011	0.059 ± 0.0040	0.050 ± 0.0030	0.048 ± 0.017
N.Ob (#)	99.25 ± 10.7 † a	86.60 ± 12.3 † a	68.20 ± 7.35 a,b	48.20 ± 8.87 b
BS/BV (%)	58.67 ± 3.88	59.07 ± 1.83	50.82 ± 4.89	58.51 ± 7.30
Ob.S/BS (%)	15.73 ± 1.52	16.57 ± 1.95	20.16 ± 2.27	13.76 ± 1.46
N.Ob/T.Ar ($1/mm^2$)	174.05 ± 11.5 †,‡ a	146.57 ± 12.0 †,‡ a	129.91 ± 14.0 a	79.05 ± 10.5 b

Table 2. Static histomorphometry parameters of bone formation. Abbreviations: T.Ar: total area; B.Ar: bone area; N.Ob: osteoblast number; BS/BV: volume-normalized bone surface area; Ob.S/BS: bone surface area-normalized osteoblast surface. N.Ob/T.Ar: number of osteoblasts per total area. Means +/= SEM. † significant main effect of genotype (WT vs. NOX4 -/-); ‡ significant main effect of EtOH (PF vs. EtOH) ($p < 0.05$, two-way ANOVA). Values with different letter superscripts are statistically different from each other ($p < 0.05$, two-way ANOVA, Student-Newman-Keuls post hoc test).

JPET Fast Forward. Published on April 13, 2018 as DOI: 10.1124/jpet.117.247262
This article has not been copyedited and formatted. The final version may differ from this version.

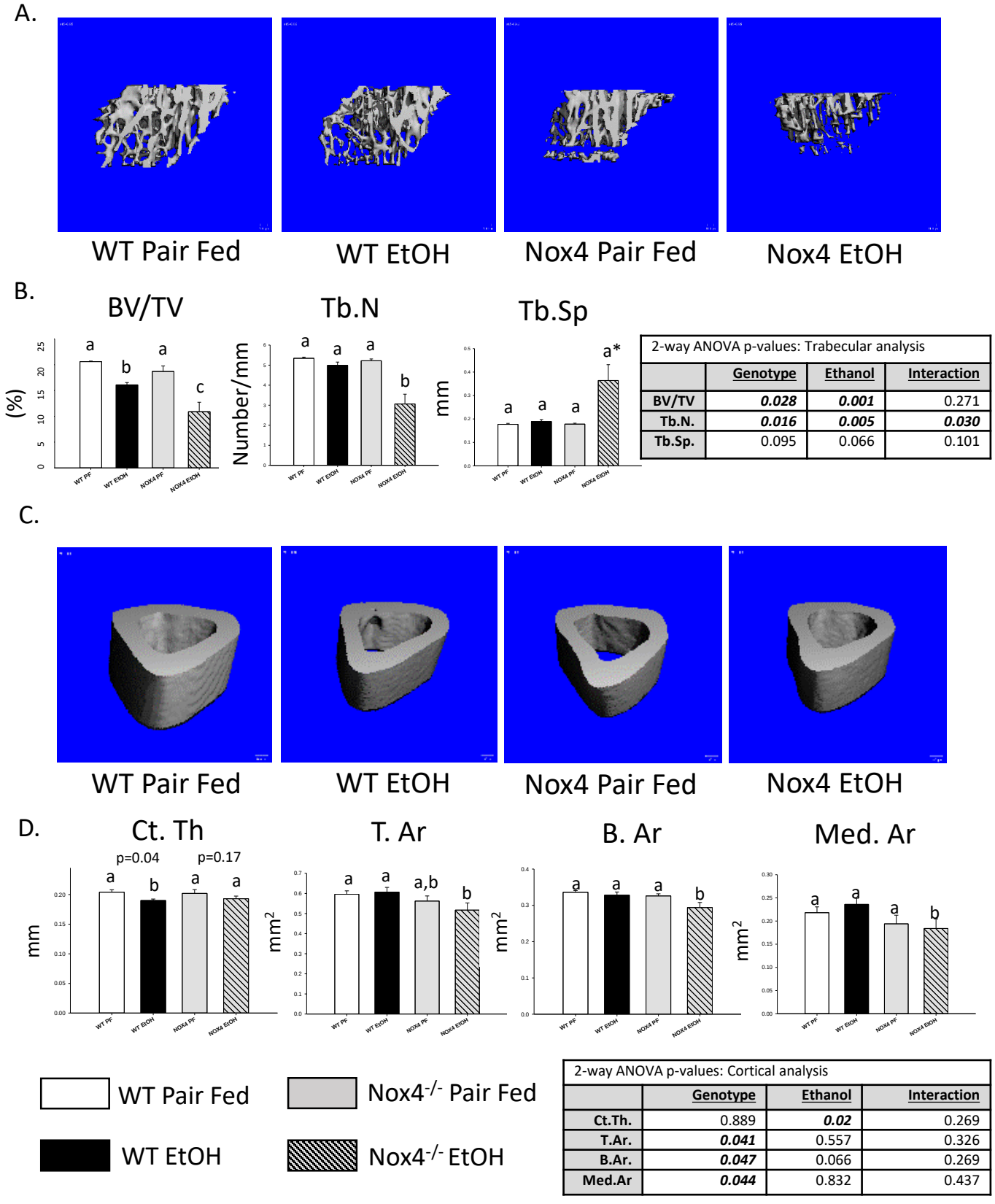

2-way ANOVA p-values: Trabecular analysis			
	Genotype	Ethanol	Interaction
BV/TV	***0.028***	***0.001***	0.271
Tb.N.	***0.016***	***0.005***	***0.030***
Tb.Sp.	0.095	0.066	0.101

2-way ANOVA p-values: Cortical analysis			
	Genotype	Ethanol	Interaction
Ct.Th.	0.889	***0.02***	0.269
T.Ar.	***0.041***	0.557	0.326
B.Ar.	***0.047***	0.066	0.269
Med.Ar	***0.044***	0.832	0.437

Figure 1.

JPET Fast Forward. Published on April 13, 2018 as DOI: 10.1124/jpet.117.247262
This article has not been copyedited and formatted. The final version may differ from this version.

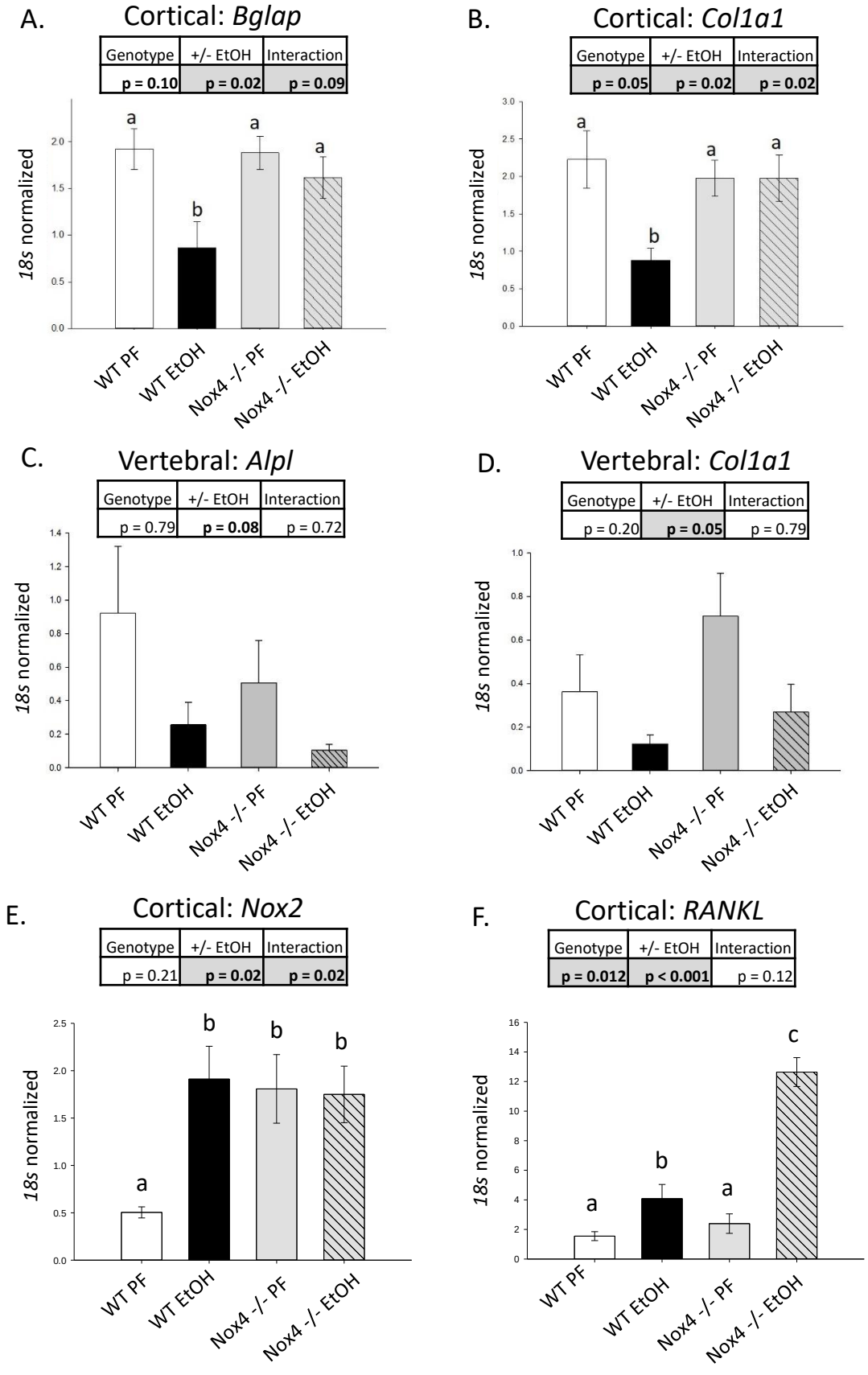

Figure 2.

JPET Fast Forward. Published on April 13, 2018 as DOI: 10.1124/jpet.117.247262
This article has not been copyedited and formatted. The final version may differ from this version.

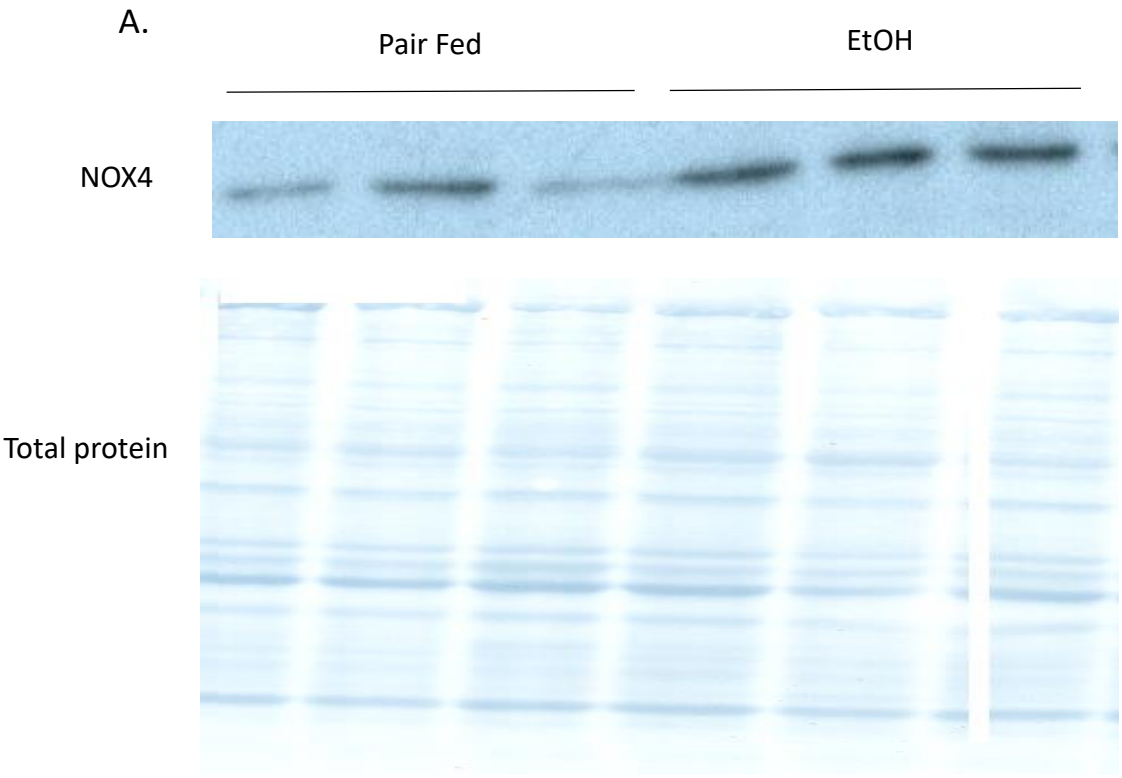

Figure 3.

JPET Fast Forward. Published on April 13, 2018 as DOI: 10.1124/jpet.117.247262
This article has not been copyedited and formatted. The final version may differ from this version.

A.

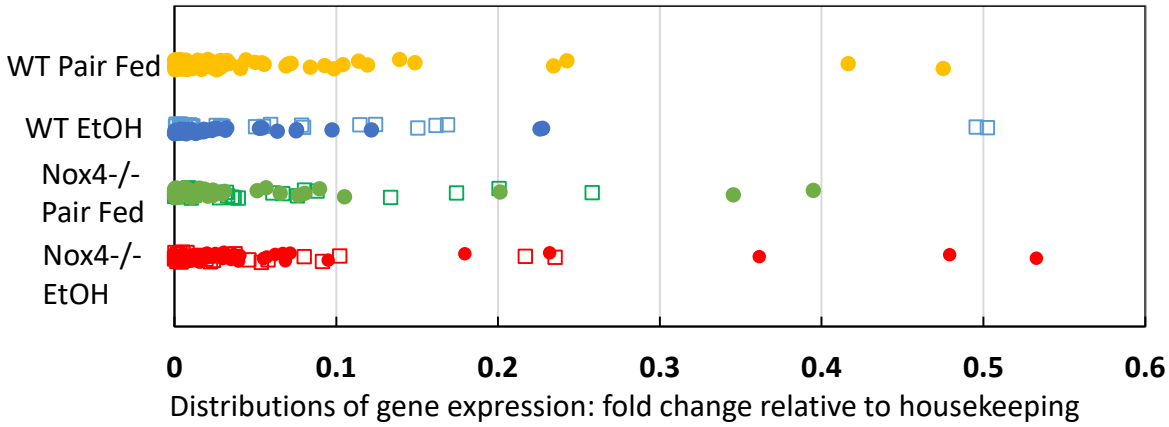

B.

Number of genes up or downregulated relative to WT Pair Fed

	☐ Upregulated	● Downregulated	Total
WT EtOH	30	48	78
Nox4 Pair Fed	34	49	83
Nox4 EtOH	38	41	79

Figure 4.

JPET Fast Forward. Published on April 13, 2018 as DOI: 10.1124/jpet.117.247262
This article has not been copyedited and formatted. The final version may differ from this version.

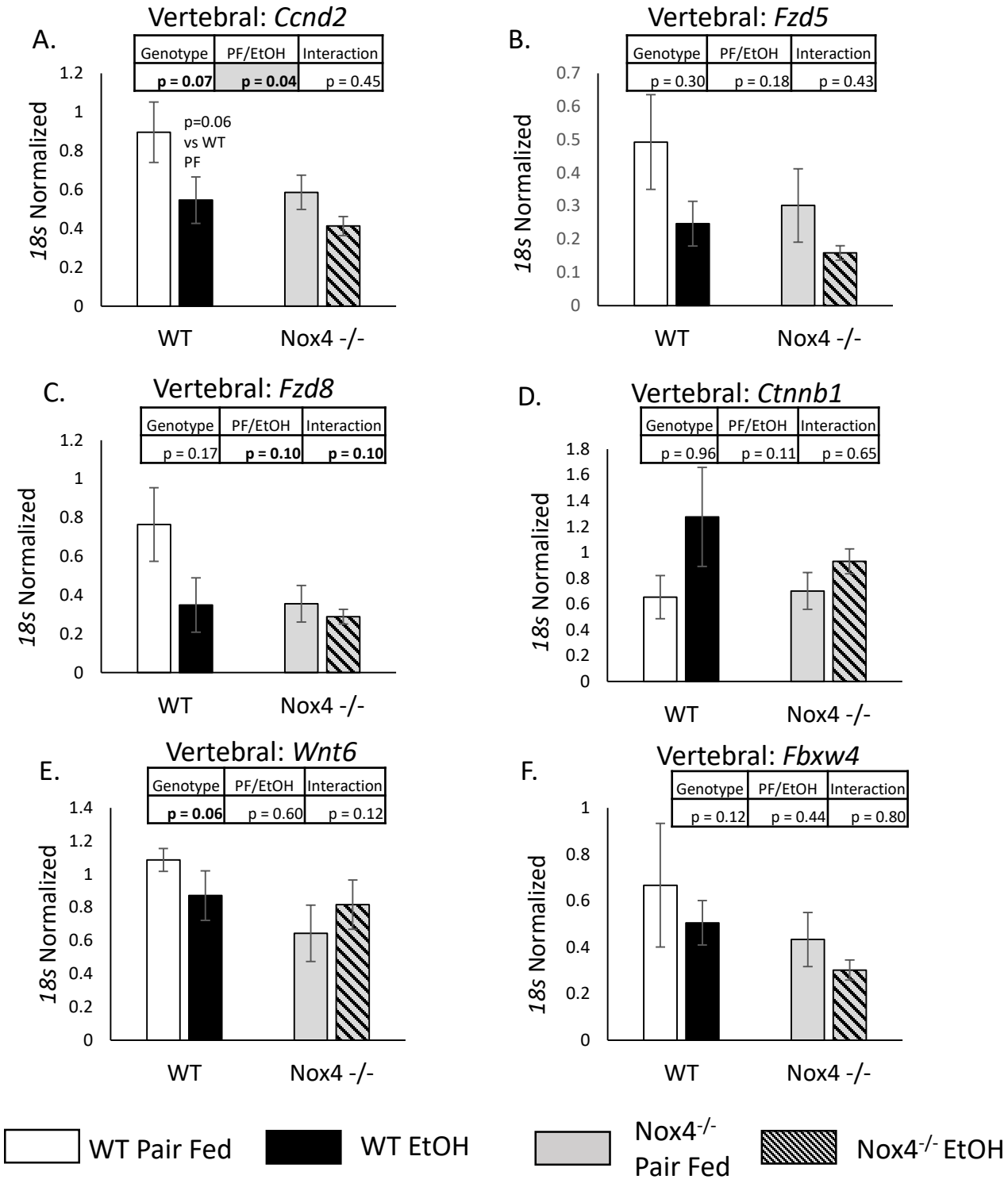

Figure 5.

JPET Fast Forward. Published on April 13, 2018 as DOI: 10.1124/jpet.117.247262
This article has not been copyedited and formatted. The final version may differ from this version.

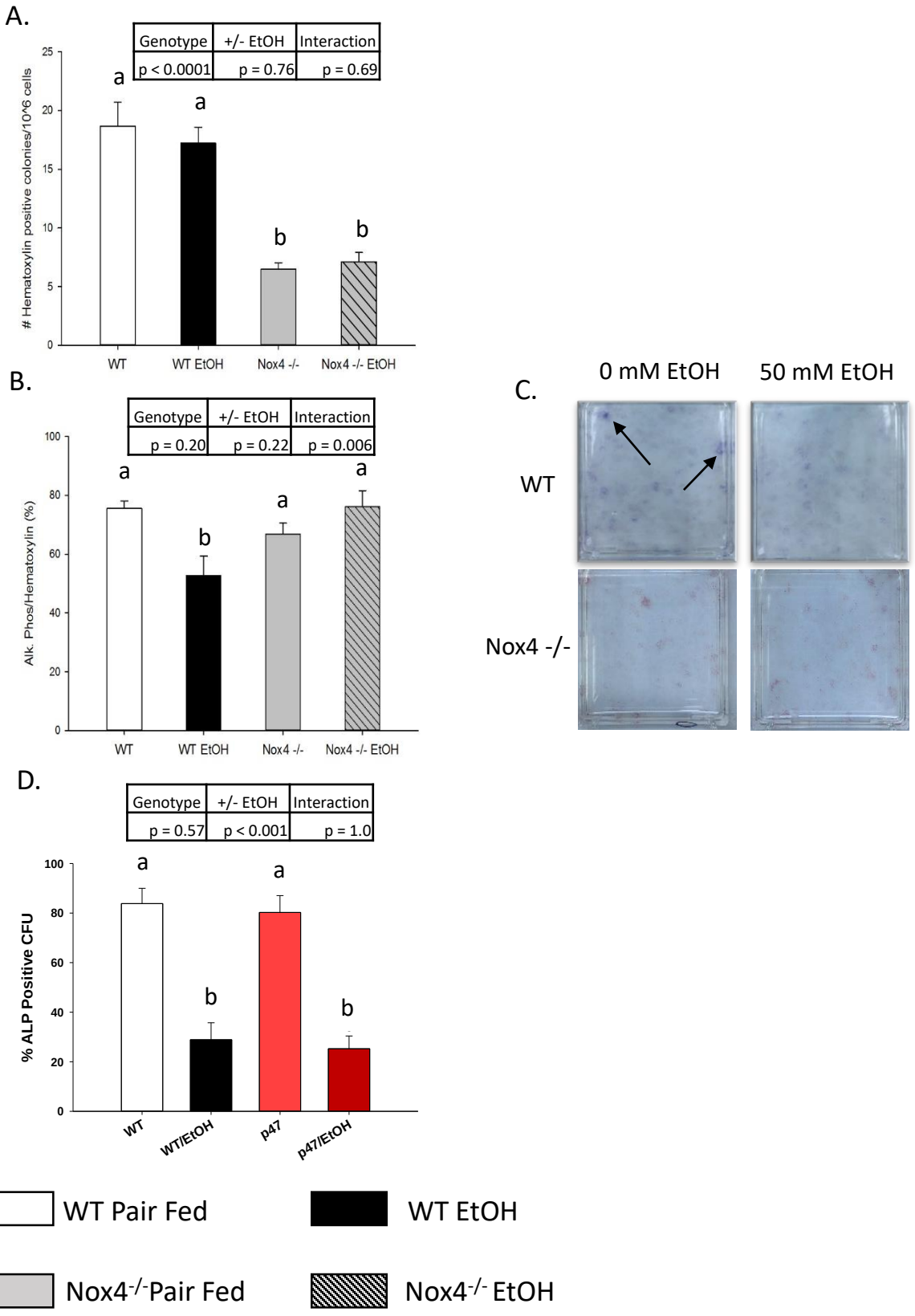

Figure 6.